Journal of Coastal Research	27	2	329–347	West Palm Beach, Florida	March 2011

Mean Circulation, Seasonal Cycle, and Eddy Interactions in the Eastern Brazilian Margin, a Nested ROMS Model

Lúcio Figueiredo Rezende[†‡], Paulo Alves Silva[‡], Mauro Cirano[§], Álvaro Peliz[††], and Jesus Dubert[‡]

[†]Universidade Estadual de Santa Cruz
45662-900, Ilhéus, Ba, Brazil
lucio@uesc.br

[‡]CESAM and Depto. de Física
Universidade de Aveiro
3810-193, Aveiro, Portugal

[§]Inst. Física
Universidade Federal da Bahia
40170-280, Salvador, Ba, Brazil

[††]Inst. Oceanografia
Universidade de Lisboa
1749-016, Lisboa, Portugal

www.cerf-jcr.org

ABSTRACT

REZENDE, L.F.; SILVA, P.A.; CIRANO, M.; PELIZ, A., and DUBERT, J., 2011. Mean circulation, seasonal cycle and eddy interactions in the Eastern Brazilian Margin, a nested ROMS model. *Journal of Coastal Research,* 27(2), 329–347. West Palm Beach (Florida), ISSN 0749-0208.

A nested configuration of the Regional Ocean Modeling System (ROMS) is used to study the seasonal circulation patterns and mesoscale activity of the Eastern Brazilian Margin (EBM). The EBM encompass an oligotrophic and bathymetrically complex zone in the NW South Atlantic from 8°S to 20°S. Sea-level anomaly data are used to validate the model. Analysis of the mean circulation reveals that the EBM is dominated by seasonal and spatial dynamics of the southward Brazil Current (BC) and the northward North Brazil Undercurrent (NBUC), as well as their connection to the South Equatorial Current (SEC) dynamics. The EBM can be divided in three dynamic provinces, which are seasonally connected either by the permanent main flow or by mesoscale process. In the northern province, from 8°S to 13°S, the NBUC is the major permanent feature and the BC is just a thin flow, confined to the top few meters. As it moves southward, the BC gets deeper and stronger. In the middle province, from 13°S to 16°S, the dominance of the top 0–100-m circulation is seasonally alternated between the southward BC flow and the northward NBUC flow. In the southern province, from 16°S to 20°S, the BC appears as a dominating surface feature. While on the top (0–100 m) the main current presents a pronounced seasonal and spatial variability, on subsurface waters (100–500 m) the NBUC connects the EBM continuously. Finally, analysis of the regional simulation reveals well-defined cyclonic and anticyclonic eddies. They detach from the main flow and translate along the domain throughout the year. The translation patterns are associated with the seasonal variability of the main EBM flow, with anticyclonic mesoscale features translating southward and mesoscale cyclonic features translating northward. On their pathway, these features may come very close to the margin, interacting with the near-shelf flow.

ADDITIONAL INDEX WORDS: *ROMS, numerical modeling, eddies and mesoscale processes, Abrolhos, Bahia, Camamu.*

INTRODUCTION

The Eastern Brazilian Margin is geographically centered along the divergence zone for the South Equatorial Current (SEC) system, in the NW South Atlantic, being subject to an intense circulation variability. Although extending over a densely populated zone and holding many diversified and important coastal marine systems, the circulation of this region is poorly understood. In this section, the geographic and oceanographic characteristics and constraints of this margin are presented, depicting the objectives of the current work.

The Eastern Brazilian Margin

The Eastern Brazilian Margin (EBM) of the NW South Atlantic (8°S to 20°S, Figure 1) has a mesotidal regime and, apart from a complex bathymetry around the Abrolhos banks (on its southern limit), presents a dominantly open and narrow continental shelf that receives moderate to low river discharges along over 30 fluvial courses (Knoppers, Ekau, and Figueiredo, 1999). Except near the major estuarine zones, a transition from siliciclastic dominant sediments in the inner shelf to pure carbonates toward the middle and outer shelves characterizes the shelf zone sedimentation along the tropical coast of Brazil (Leão, 2002). According to the *SeaWiFS* global primary productivity (U.S. Department of Commerce, 2004), the EBM is considered a Class III, low productivity ecosystem (<150 g C m^{-2} yr^{-1}). Fishing is practiced on a small scale, mostly artisanal, and catches tend to be low (Ekau and Knoppers, 2003). The EBM, therefore, presents the typical conditions of a tropical passive margin dominated by western boundary currents (Castro and Miranda, 1998).

Nevertheless, the EBM encompasses some important coastal and estuarine systems, such as Baía de Todos os Santos (BTS) and Baía de Camamu (CMU), Figure 1, where productivity is higher (although data are scant). In those systems, very distinct environmental conditions prevail. While BTS is located adjacent to the city of Salvador, a metropolitan area with over 3 million inhabitants that is affected by the pressure of intensive industrial, commercial, and fishing activity (Lessa *et al.,* 2001),

DOI: 10.2112/JCOASTRES-D-10-00059.1 received 15 April 2010; accepted in revision 26 September 2010.
Published Pre-print online 6 January 2011.

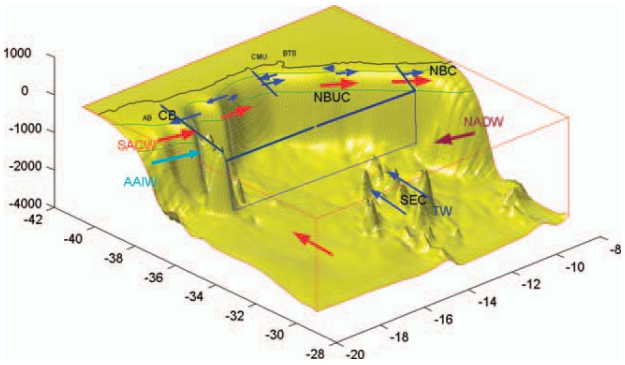

Figure 1. Schematic diagram of the main EBM flow patterns. The acronyms indicate the estimated position for the South Equatorial Current (SEC), the Brazil Current (BC), the North Brazil Undercurrent (NBUC), and the North Brazil Current (NBC). The colored vectors refer to the water masses distribution, indicating the approximate layer depth associated with the tropical water (TW), the South Atlantic Central Water (SACW), the Antarctic Intermediate Water (AAIW), and the North Atlantic Deep Water (NADW). The Abrolhos bank (AB), Baía de Todos os Santos (BTS), Baía de Camamu (CMU), and the reference transects adopted in the section "the EBM seasonal cycle" are also indicated.

CMU has its watershed surrounded by mangrove vegetation and is affected by less than 100,000 habitants distributed along a few small cities and several small-scale fisheries communities whose population is engaged in artisanal fishing (Souza and Petrere-Júnior, 2008), subsistence agriculture, and tourism activities.

Finally, on the southern EBM, the topography is marked by two major banks, the Royal Charlotte bank and the Abrolhos bank. Between those, an extended and irregular shelf projects toward the sea (the shelf width, with a mean extension around 35–45 km, widens to 110 km near the Royal Charlotte bank and to 190 km near the Abrolhos bank). Within the Abrolhos bank, from 10 to 65 km from the coast, a reef complex of approximately 6000 km^2 holds the most extensive, southernmost, coral reef aggregation in the South Atlantic Ocean (Leão, 2002). This is a spot of great biological importance, colonized by many archaic, endemic coral species, resulting from the isolation of a late tertiary community (Leão, 2002).

Owing to its physiographic character, dominantly marked by a narrow and open shelf and its diversified coastal systems, the EBM is an environmentally sensitive region. Additionally, in the past few years, there has been increasing attention on giant oil reserves struck along the Brazilian margin. Recently, 18 areas on the EBM were offered for concession, including six shallow areas, a few kilometers from Baía de Camamu. Commercial gas exploration was started in 2007 on the nearby shelf (ANP, 2009). The EBM is also vulnerable to intense tanker movement. Floating paraffin compounds, from the 2001 *Pietro Bárbaro* spill, and drift bottles released on a marine educational action were used to chart the marine currents in a pioneer effort to study the regional circulation (Rezende, 2001).

Despite extending over a zone with such great social, economic, and environmental relevance, a great uncertainty remains concerning the regional circulation patterns of the EBM and the possible connectivity between the various subsystems. Very little published science research regarding EBM dynamics exists.

The Regional Oceanography and the Scope of This Work

The most functional descriptions of the oceanographic processes in the EBM are perhaps the works of Stramma, Ikeda, and Peterson (1990) and Rodrigues, Rothstein, and Wimbush (2007). The first authors, based on a historical hydrographic data set, described the geostrophic circulation for the region, while Rodrigues, Rothstein, and Wimbush (2007) investigated the seasonal variability of the SEC bifurcation.

The SEC is a broad, westward flowing current that connects the tropical and the subtropical Atlantic Ocean through the South Atlantic subtropical gyre. Along the EBM, the SEC feeds the western boundary current system, imposing variability and determining the flow patterns. According to Rodrigues, Rothstein, and Wimbush (2007), the bifurcation latitude varies poleward with depth, while seasonally the variability is associated with changes in the local wind stress curl due to the annual excursion of the marine Intertropical Convergence Zone (ITCZ) complex. From a mesoscale perspective, the variability of the divergence, the seasonal relation between the Brazil Current (BC) and the North Brazil Current (NBC), and the interaction between the oceanic processes with the near-shelf environments are still open issues in EBM dynamics.

The major objective of this work is to establish a model view of the seasonal circulation in the EBM, retaining in the solution the connections from the large-scale circulation. The first practical difficulty that one faces when planning a regional modeling study is perhaps the establishment of a reliable annual cycle to be used as boundary conditions. The straightforward solution would be the interpolation of local data on the frontiers, but unfortunately the EBM data are scarce and irregularly sampled in time and space, as summarized by Stramma, Ikeda, and Peterson (1990), using most of the data ever surveyed for the region. Therefore, possible ways to cope with this problem, according to Penven *et al.* (2006) are (i) to have the boundary conditions provided from an independent basin scale or a global model, which according to those authors may generate doubtful consistency with the local simulation or (ii) to develop a nested grid capability, where a hierarchy of embedded, structured-grid models are able to interact between each other. In this work we adopted the second procedure, and here the regional boundary condition is provided by the coarser grid run, whose boundary conditions themselves come from a global model, with compatible resolution and processes.

Work Outline

This work was structured in seven main sections. Beyond the introduction (the first section), the nesting capability integrated into the Regional Ocean Modeling System and the modeling design is presented in the second section "The modeling design and the two nested grids." The results are presented and discussed in the third, fourth, fifth, and sixth sections "the

model validation approach," "the EBM seasonal cycle," "spatial variability and dynamic provinces," and "eddy interactions in the EBM." The first result of this work is an evaluation effort of the model itself, which is presented in "the model validation approach." The second and third parts of the results discuss the main aspects of seasonal and spatial EBM circulation patterns, which are presented in the fourth and fifth sections "the EBM seasonal cycle" and "spatial variability and dynamic provinces," respectively. In the forth and final part of the results, some of the possible interactions between the eddies, the margin, and the near-shelf processes are explored, as an attempt to establish a first-order description of the mesoscale activities revealed by the regional simulation ("eddy interactions in the EBM"). Finally, the seventh section "concluding remarks" presents a summary of the major results, emphasizing the physical aspects of the EBM temporal and spatial connectivity.

THE MODELING DESIGN AND THE TWO NESTED GRIDS

The numerical model used in this study is a primitive, nested, three-dimensional, stretched terrains–sigma following curvilinear coordinate, Regional Ocean Modeling System (ROMS) (Haidvogel *et al.,* 2000; Shchepetkin and McWilliams, 2005). ROMS applies the Boussinesq approximation and hydrostatic balance, solving the momentum equations in an Earth-centered rotating environment.

In this work a two-level, one-way nesting capability has been integrated into ROMS to obtain mesoscale solutions while preserving the large-scale circulation. The nesting downscaling was performed through the Adaptive Refinement in Fortran (AGRIF) procedure, through the ROMS-AGRIF, at ROMS Processing tools (Penven, 2003). This one-way embedding procedure has been successfully applied in various dynamic systems, such as the Peru Current System (Penven *et al.,* 2005), the Californian Upwelling System (Penven *et al.,* 2006), and the Western Iberian Shelf (Teles-Machado *et al.,* 2007), among many others.

A regional grid of 1/12°, here named the mesoscale grid (MG), spanning approximately from 8°S to 20°S and from 29°W to 40°W, was nested on the larger scale grid (1/4°), referred to as the large grid (LG), encompassing a larger domain of the Western South Atlantic Ocean, from 5°N to 35°S and from 10°W to 55°W (Figure 2). Since the near-shore currents have a spatial scale of 1–30 km, while the offshore dynamics has a spatial scale of 30–100 km, the MG (~9-km grid cell resolution) is then capable of solving the mesoscale dynamics connecting the near shore, the shelf, and the ocean basin, while the LG (~27-km grid cell resolution) is intended to solve the large-scale dynamics.

The model was initialized with Levitus climatology and forced by climatological monthly winds, heat, and fresh water fluxes from the Comprehensive Ocean-Atmosphere Data Set (COADS; Da Silva, Young, and Levitus, 1994), running for a 15-year period. The strategy adopted was to run the LG grid alone for the first 10 years and then to have the one-way nesting procedure implemented for the following 5-year run. The LG uses radiational, active, implicit, open boundary conditions, where the solution at the boundary is nudged toward dated monthly mean outputs (1990 to 2004) of the

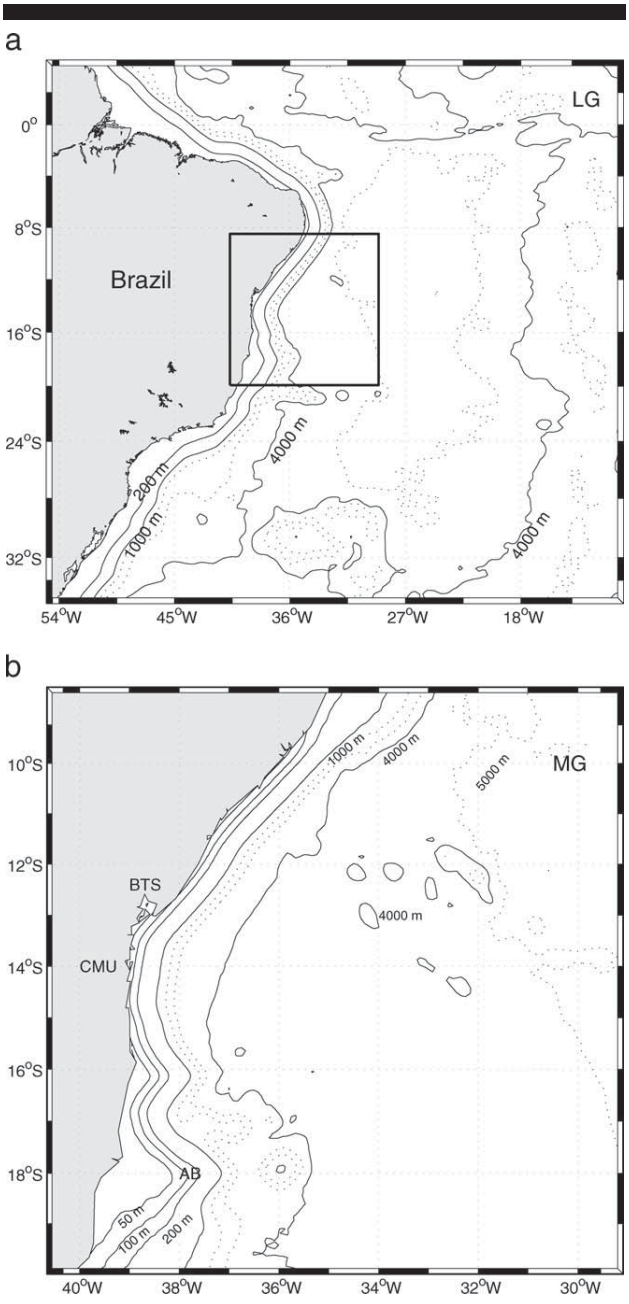

Figure 2. ROMS nested grid system and bathymetry used: (a) Large Grid (LG) and (b) Mesoscale Grid (MG). Solid lines represent the 50- (MG only), 100- (MG only), 200-, 1000-, and 4000-m isobaths. The 2000-, 3000-, and 5000-m isobaths are represented as dotted lines.

Simple Ocean Data Assimilation (SODA) reanalysis (Carton *et al.,* 2000; Carton, Chepurin, and Cao, 2000). The lateral boundary conditions for the MG were provided by the LG grid. Explicit lateral viscosity is null in the entire domain except at the sponge layers (the closest six grid lines from the boundary), where it increases smoothly to a value of 1000 $m^2 s^{-1}$ for LG and 330 $m^2 s^{-1}$ for MG. A nonlocal, K-profile planetary boundary

Table 1. *Model configuration parameters.*

	LG	MG	
Parameter			
L	179	138	Pts. in longitude direction
M	169	141	Pts. in latitude direction
ΔS	1/4°	1/12°	Horizontal resolution
Δt	1800 s	600 s	Baroclinic time step
Δt_f	40 s	13.3	Barotropic time step
Common Parameters			
N	30		Number of s levels
Θ_s	6.0		Sigma coord. stretch factor
D	10.0 m		Minimum model depth
R	$3.0 \times 10^{-4}\,\mathrm{m\,s^{-1}}$		Linear bottom drag coeff.

layer scheme (Large, McWilliams, and Doney, 1994) parameterizes the sub–grid-scale vertical mixing processes.

The bottom topography was interpolated from ETOPO2-2′ gridded global relief data (U.S. Department of Commerce, NOAA, 2001) for both grids, and, where necessary, it was smoothed to fit the bathymetric gradient to a maximum slope factor ($r = \Delta h/(h_1 + h_2) \cong 0.2$) in order to prevent pressure gradient errors associated with the sigma coordinate system (Haidvogel *et al.,* 2000). Table 1 summarizes the model configuration for LG and MG grids.

THE MODEL VALIDATION APPROACH

The basis of validation is to assess a model response by comparing the output to physically measured data, such as currents, hydrography, or mesoscale variability. Mesoscale variability is a major characteristic of ocean dynamics and may be estimated with global coverage altimetric data (Brachet, Le Traon, and Le Provost, 2004). A validation of the LG model results with altimetric-derived mesoscale variability is presented on the sections "eddy kinetic energy" and "sea surface height anomalies." This procedure assumes a special interest regarding the paucity of *in situ* data available (Backeberg, 2006). Further on, the large-scale circulation patterns based on historical observations and in model results are presented in the section "oceanographic characteristics based upon historical observations and model," while a comparison of selected modeled transport with *in situ* measured values from the literature is presented in the section "transport estimates."

Eddy Kinetic Energy

The ocean mesoscale variability was estimated based on the eddy kinetic energy (EKE), calculated from *TOPEX/Poseidon*, *ERS-1/2*, and *Jason* combined data for sea-level anomaly (SLA), obtained from the archiving, validation, and interpretation of satellites oceanographic (AVISO; Ducet, Le Traon, and Reverdin, 2000). Since mesoscale structures present typical time-space scales of 10 to 100 days and 50 to 500 km, the merging of multiple altimeter data on the AVISO data set allows for a realistic sea-level and geostrophic velocity calculation, resulting in a good quality mesoscale observation (Ducet, Le Traon, and Reverdin, 2000). The altimeter SLA data used cover a 5-year period, from January 2000 to December 2004, and present a 1/3° spatial resolution.

The analyzed model data also cover a 5-year period of sea surface height (MSSH), and each output represents an average over a 10-day period. The model eddy kinetic energy was estimated from the model sea-level anomalies (MSLA), using a similar procedure to the altimeter data preprocessing. The MSLA was computed from MSLA = MSSH − $\overline{\text{MSSH}}$, where the bar represents a mean over the 5-year period. Only the larger scale grid simulation, which has a similar spatial resolution to altimetric data, was used in this analysis.

Both altimetric (SLA) and the model (MSLA) were used to compute the surface zonal (Ug') and meridional (Vg') velocity anomalies, using the geostrophic approximation:

$$Ug' = \left[-\frac{g}{f}\left(\frac{\partial \eta}{\partial y}\right)\right] \tag{1}$$

$$Vg' = \left[-\frac{g}{f}\left(\frac{\partial \eta}{\partial x}\right)\right] \tag{2}$$

where g is the gravity acceleration, f is the Coriolis parameter, and $\partial\eta/\partial x$ and $\partial\eta/\partial y$ are the meridional and zonal gradients of SLA and MSLA. The variance of the velocity anomaly field corresponds to the eddy kinetics energy (EKE):

$$EKE = \left[\frac{1}{2}\left\{(Ug')^2 + (Vg')^2\right\}\right] \tag{3}$$

Figure 3 (left panels) present the mean EKE distribution for altimetry (top) and ROMS (bottom) along the LG domain, while Figure 3 (right panels) presents a zoom of the same distribution on the EBM region. Maximum values of EKE are found on the energetic, equatorial zonal circulation. Minimum values are found on the oceanic region located between 8°S to 24°S. In the EBM, an EKE intensification occurs on the outer shelf vicinity, reflecting the high variability of the western boundary dynamics associated with the northward flow of the NBC system and the southward BC flow. South of this region, the LG domain shows the BC flow, marked by relative high EKE variability along the southern coast of Brazil. Secondary EKE peaks, with values >300 $\mathrm{cm^2\,s^{-2}}$ are seen around 35°S, marking the confluence of the BC with the northward flow of the Malvinas Current system (Saraceno *et al.,* 2004).

In order to have a zonal view of the EKE results, we have also computed the mean zonal EKE (Figure 4). This zonal estimate was obtained by time and space averaging the EKE results, from the 200-m isobath to 30°W, in one degree steps (7(±0.5)°S to 35(±0.5)°S), focusing on the western basin signal. The lower latitude EKE signal was omitted, since geostrophy breaks down near the Equator.

Overall, ROMS captures the spatial EKE distribution with reasonable confidence but tends to underestimate the ocean variability toward the northern (*e.g.,* the energetic equatorial circulation zone) and the southern grid extensions (*e.g.,* the Brazil–Malvinas confluence zone). An extended LG domain could possibly reduce this effect but also increase the computational time. Along the EBM, ROMS captures the larger energy associated with the western boundary currents but shows larger variability and higher mean EKE, which could be partially ascribed to

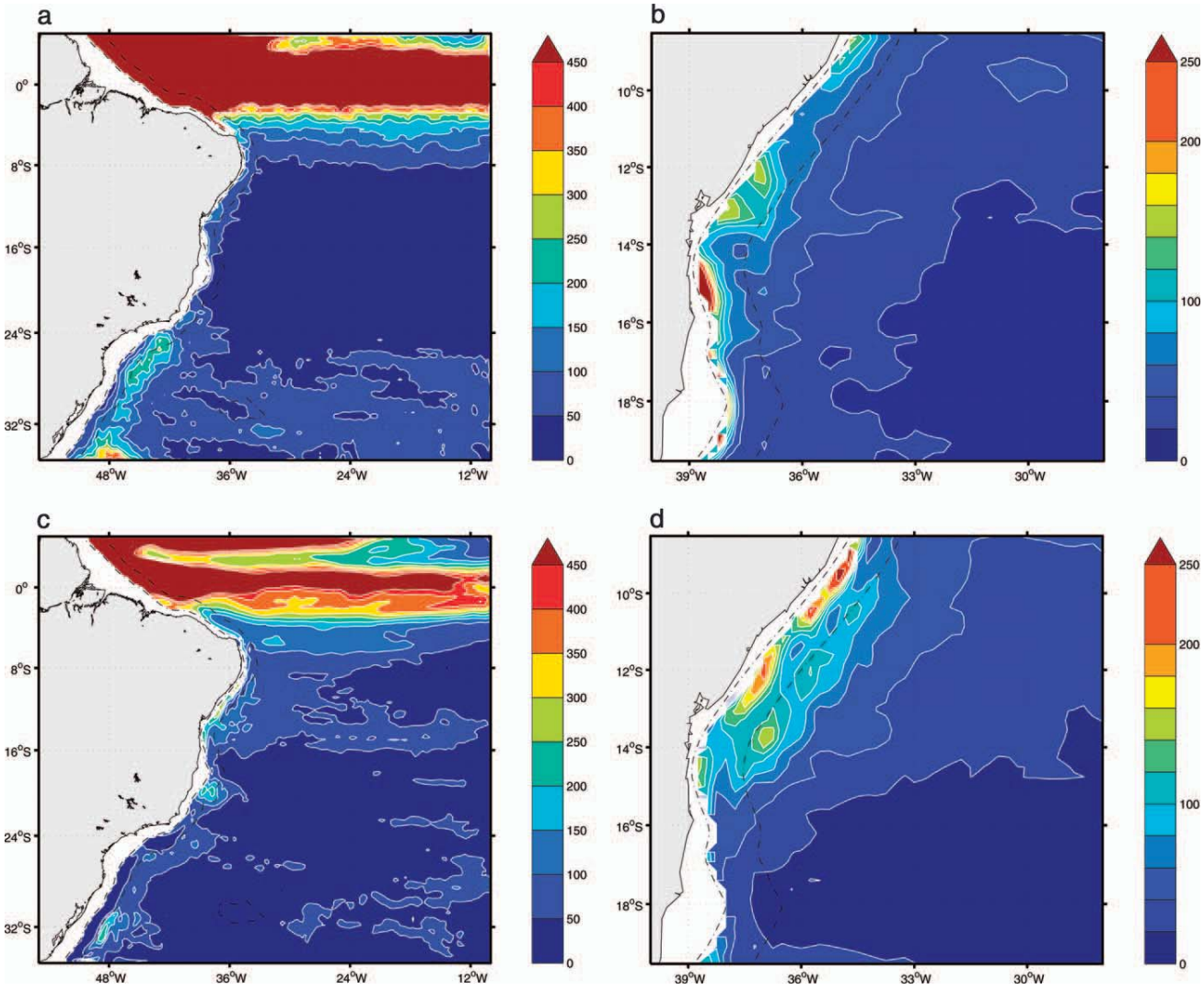

Figure 3. Mean EKE ($cm^2\ s^{-2}$) in the western South Atlantic (left) and detailed representation in the Eastern Brazilian Margin (right). The top panels represent the altimeter and the lower panels represent ROMS. Dashed lines represent the 200- and 2000-m isobaths. Color scale is broken for values 450 $cm^2\ s^{-2}$ (left) and >250 $cm^2\ s^{-2}$ (right).

the remaining differences in the spatial resolution between ROMS and the altimetry.

The evaluation of the EKE was also used to obtain an optimal model configuration. Prior experiments were established with alternative boundary and forcing data sets. The results (not shown) revealed less intensity and larger discrepancy in the model EKE, especially on the EBM region, justifying our option for the SODA boundary conditions and COADS wind forcing and fluxes, whose comparative results showed better convergence.

Sea Surface Height Anomalies

The austral summer and winter mean distribution for sea surface height anomalies (SSHA) is presented on Figure 5 for the Altimeter (left) and ROMS (right) along the Western South Atlantic. A similar procedure was used by Penven *et al.* (2005) to validate ROMS along the Pacific coast of Peru.

Higher anomalies are noticeable above the Equator and bordering the outer shelf, south of 10°S. For the latter case, the elongated outer shelf feature is associated with the intensification of the coastal upwelling events during summer, enhancing the negative anomalies. During winter, the prevalent SE winds regime increase the Ekman transport toward the coast, intensifying the positive anomalies.

Major differences between the SSHA and the model are found in the region comprised from 2°N to 4°S, east of 24°W during winter. Altimetry suggests that SSHA is much reduced in that region, but such behavior is not seen in ROMS. This may

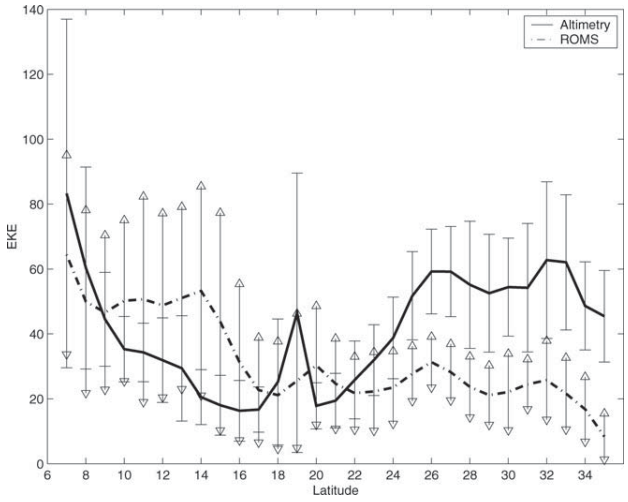

Figure 4. Mean zonal EKE distribution ($cm^2\ s^{-2}$) from altimeter and ROMS. Error bars represents the standard deviation from the mean.

be related to the failure of ROMS to reproduce some features of the equatorial circulation due to imposition of artificial boundaries in its vicinity. At latitudes higher than 30°S, the anomalies show a very irregular pattern, with an increase of variability values at the Brazil–Malvinas confluence zone. Despite certain discrepancies, ROMS is able to capture the SSHA seasonality and presents a reasonably good spatial agreement with the altimeter data, particularly along the EBM.

Oceanographic Characteristics Based upon Historical Observations and Model

From ROMS LG model results, the general circulation patterns in the Western South Atlantic evolve from a zonal regime, typical for the equatorial dynamics, to a more irregular oceanic regime toward higher latitudes (Figure 6). The circulation in the EBM is remarkably influenced by the SEC bifurcation. The SEC is a broad, westward flowing current that connects the tropical and the subtropical Atlantic Ocean through the South Atlantic subtropical gyre. As the southern branch of the SEC approaches the EBM, carrying subtropical Benguela Current water toward the shelf, it bifurcates into the northward flowing North Brazil Undercurrent (NBUC) and the southward flowing BC (Stramma, Ikeda, and Peterson, 1990; Stramma and Schott, 1999).

According to Rodrigues, Rothstein, and Wimbush (2007), the annual bifurcation position varies poleward with depth, from 10°S to 14°S near the surface to 27°S at the 1000-m depth. On the top 200 m, the bifurcation reaches its southernmost position in July (~17°S) and its northernmost position in November (~13°S). On the upper thermocline, the bifurcation variability is associated with changes in the local wind stress curl due to the annual N-S excursion of the marine ITCZ complex (Rodrigues, Rothstein, and Wimbush, 2007)

The NBUC is the component of the North Brazil Current System that, occupying the top 1000 m of the water column, flows along the NE coast of Brazil, up to the Cabo de São Roque (~5°S). From this point, as it flows NW toward the Equator, the NBUC receives an additional inflow from the SEC, becoming an intensified surface current known as the NBC (Schott, Fischer, and Stramma, 1998).

On the surface (0–100 m) layer (Figure 6a), the model captures the position and magnitude of a northward surface flow, associated with the NBC system (north of 12°S) and a southward flow, associated with the BC system, south of 12°S. Close to the SEC bifurcation, both current systems carry the oligotrophic and warm tropical water (TW), brought by the SEC.

While the NBC is an intense western boundary current and the dominant surface circulation feature in the western tropical Atlantic Ocean (Silveira, Miranda, and Brown, 1994), the BC is a weak and shallow western boundary flow (*e.g.,* Evans, Signorini, and Miranda, 1983), carrying the oligotrophic, warm and salty TW ($T > 20$°C and $S > 36$) (Emilsson, 1961). As the BC reaches subtropical latitudes it becomes deeper and gradually incorporates the nutrient richer, colder, and fresher South Atlantic Central Water (SACW, 6°C $< T <$ 20°C and $34.6 < S < 36$; Miranda, 1985). Reid (1989) defines this SACW southward flow to be found at latitudes south of 20°C.

At the subsurface (100–500 m) layer (Figure 6b), the SEC bifurcation, which at this layer transports SACW, is captured by the model between 16°S to 20°S. Along the EBM, the northward NBUC flow appears as the most prominent dynamic feature.

In our model, most of the top (0–500 m) EBM is characterized by an opposing flow, where the southward surface flow, associated with the BC, is opposed to a northward flow, underneath, associated with the NBUC. The BC appears as a relatively weaker flow that runs along the Brazilian coast and gets stronger beyond 24°S. At latitudes north of 10°S the NBUC merges with the surface flow and the NBC system emerges, appearing as an intensified NW flow, moving beyond the Equator.

Below the SACW layer, there are two major water masses, the Antarctic Intermediate Water (AAIW) and the North Atlantic Deep Water (NADW). Both layers present a well-defined circulation in our model. North of 25°S, and apart from some recirculation, the AAIW layer flows toward the Equator. Stramma and England (1999) center the SEC bifurcation at the AAIW layer south of 25°S. The model flow at the NADW layer reveals a continuous southward flow and, again, a significant recirculation at the EBM, probably a reflection of the complex margin bathymetry. Although we do not further discuss the results for the deeper layers, the general flow pattern reported in the literature (*e.g.,* Stramma and England, 1999; Silveira *et al.,* 2000; Cirano *et al.,* 2006; Rodrigues, Rothstein, and Wimbush, 2007) are captured by the model.

Moreover, considering the nesting capability, the LG and MG solutions exhibited a similar vertical structure. For comparison, the mean zonal section at 14°S for January is represented in Figure 7 for both grids. On the top 1500 m, they simulate a well-defined western boundary flux, with the BC being represented by a southward surface flow extending to about 150 m on the shelf/slope region. Below this surface flow, the most prominent feature is the northward flowing SACW and

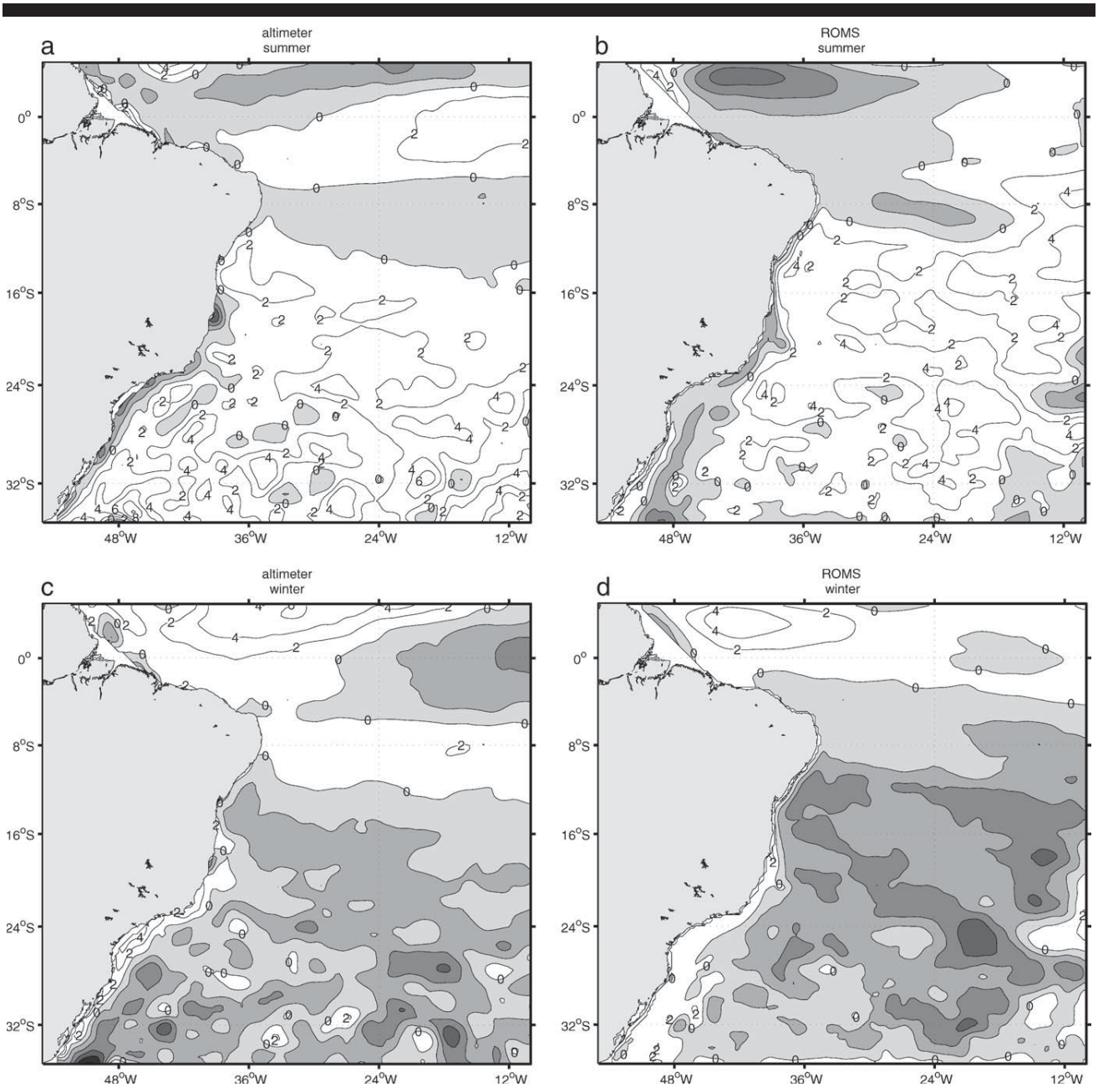

Figure 5. Summer and winter mean sea surface height anomalies for altimeter (left) and ROMS (right). Shading represents negative anomalies. The contour interval is 2 cm.

AAIW, which extends from 200 m to about 1500 m. It is interesting to notice that, at depths deeper than 1500 m, the MG solution shows a less intense and more realistic southward NADW flow (velocities around 0.1 m s^{-1}), not underneath the AAIW flow, but with some displacement to the east. Although both solutions resemble a similar structure, the MG presents a more detailed and accurate vertical flow distribution than the LG results, reflecting the more realistic bathymetric outline and the efficiency of the nesting procedure.

Transport Estimates

In order to compare the modeled transport results with observation, we summarized some typical EBM transport values from the literature in Table 2. Most of the existing values are based on geostrophic estimates from historical and highly spaced hydrographic data, presenting a qualitative view of the flow but possibly biasing narrow flows, such as the intense NBUC flow, whose core is confined to a width of less

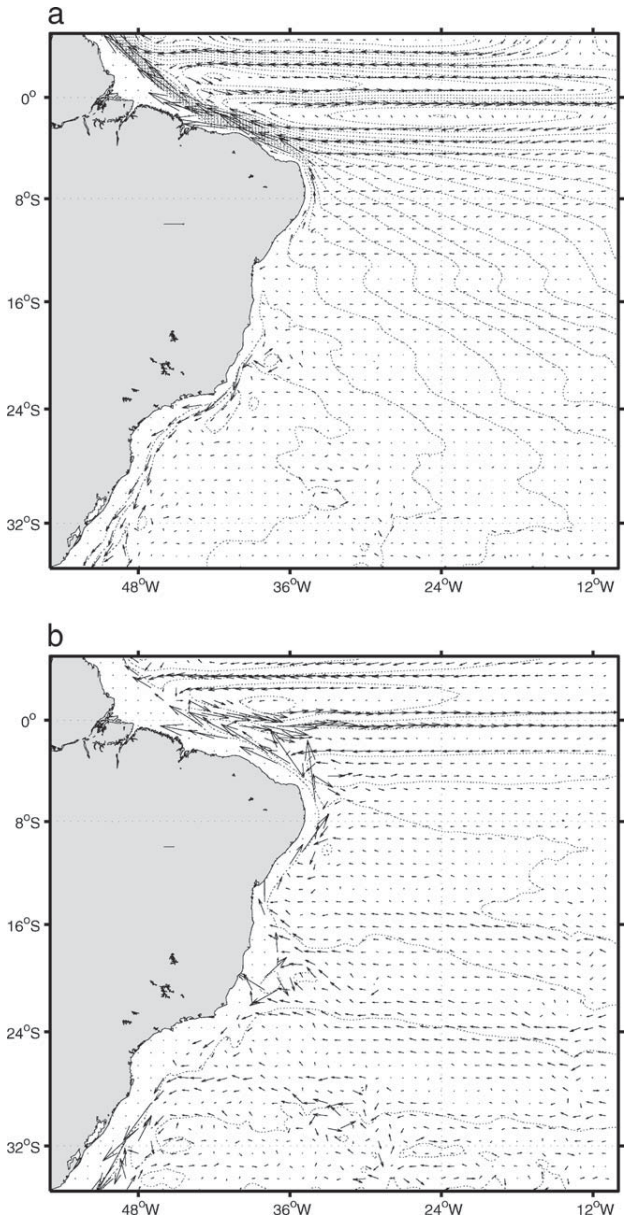

Figure 6. Annual mean flow (vectors) and stream function (isolines) in the western South Atlantic integrated for the layer: (a) 0–100 m and (b) 100–500 m, LG model results. The vector scale is (a) 0.4 m s^{-1} and (b) 0.2 m s^{-1}.

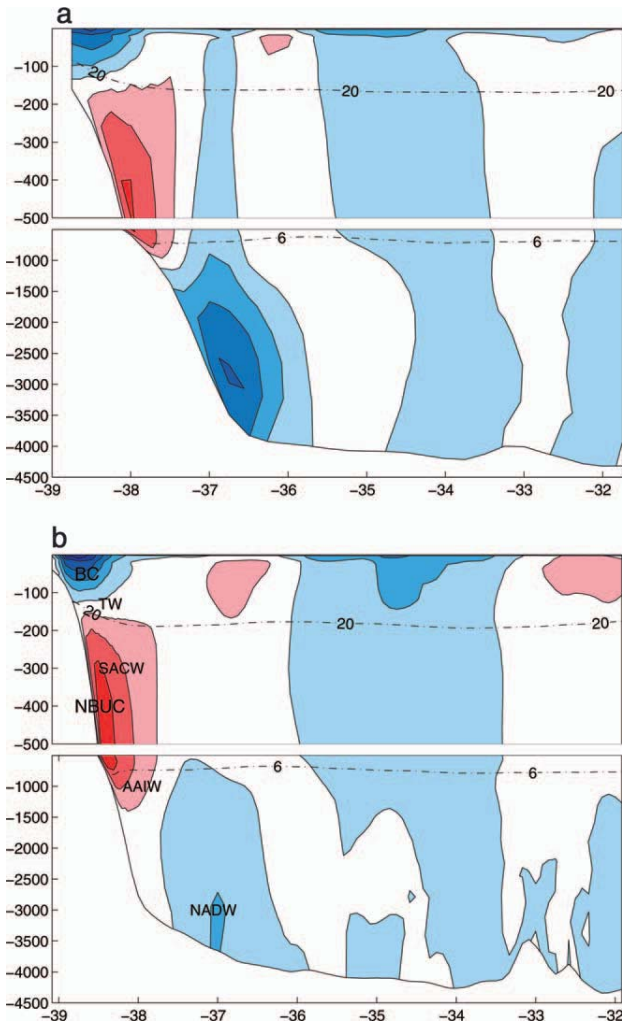

Figure 7. Vertical section at 14°S of the modeled mean meridional velocity from (a) LG and (b) MG, in January. Red (blue) shades represent positive northward (negative southward) flow. The isotherms of 20°C and 6°C indicate the interfaces between TW/SACW and SACW/AAIW, respectively. The contour interval is 0.1 m s^{-1}, and the acronyms are indicated in Figure 1.

than 100 km along most of the EBM (Figure 7). Nevertheless, geostrophic estimates are still a reference for model validation in spite of a few direct measurements made in the upper EBM (Table 2).

Schott *et al.* (2005), based on current meter array series, found a mean transport of 15.3 Sv for the upper NBUC at 11°S. Based on five Lowered Acoustic Doppler Profiler (LADCP) ship transects, the same authors also found a mean transport of 13.5 Sv at the ($\sigma_\Theta < 26.8$) layer section, west of 31.5°S (Table 2). These values are compatible with our model result of 14.2 Sv for the northward annual transport for the layer 0–400 m at 11°S (not shown) and higher than the geostrophic estimate of 4.7 Sv at 10°S and the 5.7 Sv geostrophic estimate for the 9°–13°S transect, presented by Stramma, Ikeda, and Peterson (1990).

For the remaining EBM, no direct measurements have yet been published. Stramma, Ikeda, and Peterson (1990) estimated a southward transport of 2.1 Sv, for February, at 15°S (Table 2). Our 0–100-m model value, at 14°S, reveals an annual net value of 0.5 Sv, with a seasonal intensification trend toward summer. In this surface layer, where most of the BC transport occurs, and specifically for February, we found a comparable net transport of ~2.0 Sv (not shown).

At 18°S, both model and geostrophic estimates reflect the dominance of the BC on the surface flow. Miranda and Castro (1982) estimated the BC transport to be of 6.5 Sv, with most of it

Table 2. *Observed meridional transport (Sv) along the Eastern Brazilian Margin. When the transport is based on geostrophic calculation, the reference level is indicated. Negative values indicate a southward transport. 1 Sv = 10^6 m^3 s^{-1}.*

Longitude/ Transect Long.	Depth Ref.	Data Period	Transp. (Sv)	Flow System/Layer	Reference
10°5′/30°1′W	390–500 m	Feb. 1975	4.7	Transect	1
11°S	Moored	Mar. 2000 to Mar. 2004	15.3	Upper NBUC/~(0–400 m)	2
	Current Meter		10.4	Lower NBUC/~(0–400 m)	
11°S	ADCP/LADCP	Mar. 2000 to Aug. 2004	1.6	NBUC/$\sigma_\theta < 24.5$	2
			12.9	NBUC/$24.5 \le \sigma_\theta < 26.8$	
			10.9	NBUC/$26.8 \le \sigma_\theta < 32.15$	
9°–13°S/30°W	390–510 m	Sep. 1926	5.7	Transect	1
15°S/29°59′W	470–530 m	Feb. 1975	−2.1	Transect	1
19°S	130 cl ton^{-1} (~520 m)	Sep. 1967	−6.5	BC	3
19°S/30°05′W	560–670	Sep. 1967	−0.8 (−3.7)	Transect (BC)	1
19°S	500 m	Apr. 1982	−5.3	BC	4
19°25′S	470–640 m	Jun. 1970	−5.7	BC	1
19°30′S	480–560 m	Mar. 1957	−1.0	BC	
20°03′S	590–630 m	Jan. 1975	−1.9	BC	

References: (1) Stramma, Ikeda, and Peterson (1990); (2) Schott *et al.* (2005); (3) Miranda and Castro (1982); (4) Evans, Signorini, and Miranda (1983).

occurring on the first 200 m. Stramma, Ikeda, and Peterson (1990), using a similar data set (a closer sampled transect from September 1967) with a slightly different reference level, found a southward net transport of 0.8 Sv, for the section west of 30°S, and a BC estimate of 3.7 Sv, suggesting an intensive opposing flow along the section. Other estimates (Table 2) show the BC transport varying from 1.0 to 5.3 Sv. Our model presents an annual mean of 2.8 Sv for the surface layer (not shown).

THE EBM SEASONAL CYCLE

In order to investigate the seasonality of the circulation on the EBM, we analyzed monthly mean results for MG, calculated over a 5-year period and based on 10-day average outputs. Focusing on the western boundary dynamics, zonal sections were established at the center of the region (14°S) and symmetrically on the northern (10°S) and southern (18°S) extensions of the domain. A meridional section was also established along 34°W meridian, in order to evaluate the SEC transport into the system. The sections are illustrated in Figure 1.

The spatial and temporal variability on the EBM meridional flow through these three sections is synthesized in Figure 8, which shows the vertical structure for January, April, July, and October at these sections. The isotherms of 20°C and 6°C indicate the interfaces between TW/SACW and SACW/AAIW, respectively. Figure 8 shows that the EBM is subject to a marked spatial character and an intense seasonal variability. For instance, the south flowing BC appears as a seasonal flow (January and October) confined to the top few meters at 10°S and as a deeper and permanent flow at 18°S. This flow is stronger toward the austral summer. On the other hand, the north flowing NBUC appears as a permanent feature along the entire domain, getting stronger and merging with the surface flow at the northern section. The NBUC transport peaks toward the middle of the year. Quantitative transport estimates provide the basis for a EBM dynamics characterization, which is described next.

Considering that our main interest is the shelf-slope region, the meridional volume transport was calculated on each section, from the coast to the eastern limit of the main flow, which lies approximately at the 4000-m isobath. Therefore, at 10°S, the transport section was set between 34°W to 36°W; at 14°S, between 37°W to 39°W; and at 18°S, between 35°W to 39.5°W. The wider section at 18°S is due to an extended continental shelf, a factor that determines a less confined surface flow on that latitude. Although the calculated transport is dependent on the extension adopted, and that does not adhere to a very strict criteria, we have observed that by promoting small variations on the length of the sections, the relation between the fluxes tends to remain constant. The mean meridional transport values are presented for both components of the flow and are separated in two vertical layers, here named surface (0–100 m) and subsurface (100–500 m).

To evaluate the onshore transport entering the EBM, mostly through the SEC flow, the zonal transport was calculated in two segments along 34°W, a northern segment from 10°S to 14°S and a southern segment from 14°S to 18°S. For these meridional sections, we present the net transport integrated over the two vertical layers defined above.

Based on the analysis of the transport summarized in Figure 9 (left panels), we observe that at the surface layer, the southward transport presents a flow increment toward higher latitudes, with mean annual values of 0.5 Sv (10°S), 2.4 Sv (14°S), and 2.8 Sv (18°S). The annual surface transport is dominantly toward the north, at 10°S, with a net transport of 2.7 Sv, and dominantly toward the south at 18°S, with a net transport of 1.0 Sv. This suggests that the BC appears as the dominant surface boundary current at 18°S, while at 10°S, the NBC/NBUC system is the main dominant surface feature. At the middle section, 14°S, the resultant annual surface transport (net of 0.4 Sv) is slightly toward the south. The seasonal pattern, however, suggests an alternate dominance of the circulation throughout the year.

At the subsurface layer (Figure 9, right panels), the northward flow is clearly dominated by the NBUC transport, carrying SACW toward equatorial regions. This transport presents an increment of 6.6 Sv, varying from 8.5 Sv at 18°S to 15.1 Sv at 10°S. A steady latitudinal transport increment is

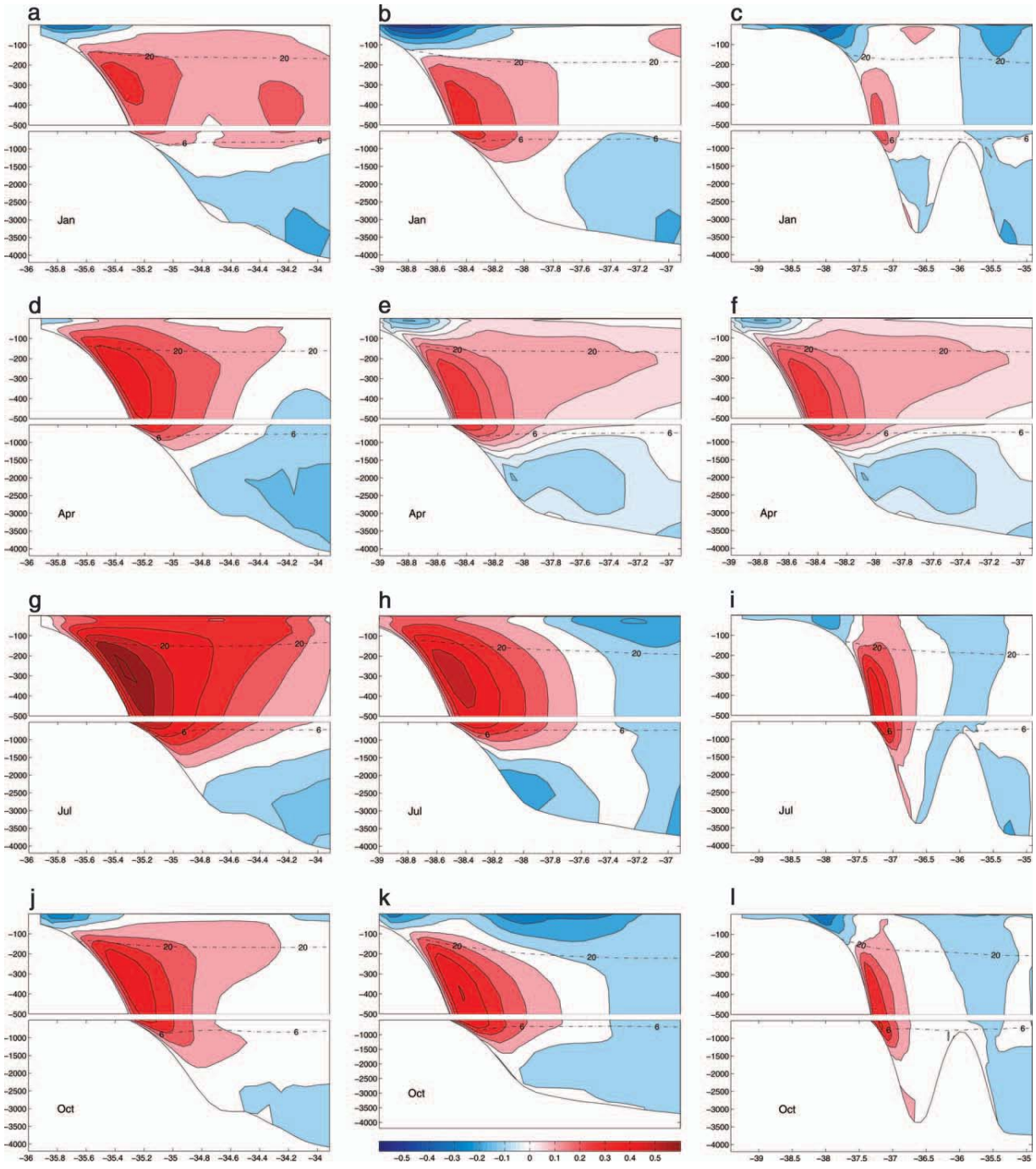

Figure 8. Mean meridional velocity at 10°S (left), 14°S (middle), and 18°S (right) for selected months, from top to bottom: January, April, July, and October. Red (blue) shades represent positive northward (negative southward) flow. The isotherms of 20°C and 6°C indicate the interfaces between TW/SACW and SACW/AAIW, respectively. The contour interval is 0.1 m s^{-1}.

observed on the southward transport. In general, the southward subsurface transport is lower than the surface layer transport (Figure 9, left panels), except at 18°S, where it gets slightly stronger, indicating a deepening of the BC flow toward higher latitudes. The net transport at the subsurface layer is always northward oriented, presenting an increment of 9.1 Sv from the southern section to the northern section.

At 10°S, the NBC/NBUC is the dominant dynamic feature. The annual variability of the transport presents a similar behavior between the surface and the subsurface layers and a marked

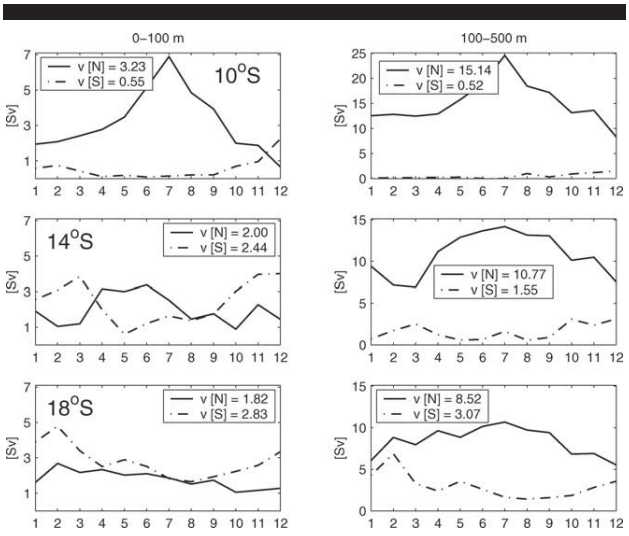

Figure 9. Annual cycle of the monthly mean transport (Sv) estimates along the zonal sections at 10°S (top panels), 14°S (middle panels), and 18°S (bottom panels). Northward (southward) transport is positive (negative). The left panels represent the surface layer (0–100 m) and the right panels represent the subsurface layer (100–500 m). The annual mean transports for each direction are indicated inside the boxes. 1 Sv = 10^6 m^3 s^{-1}.

seasonal signal. The peak transport occurs in July and is coherent with the largest zonal inflow at 34°W presented in Figure 10. The southward flow, which for most of the year transports under 1 Sv, also presents a marked seasonality, reaching a peak of 2 Sv at the end of the year. Whether such transport could be ascribed to the origin of the BC is still an open question.

By applying an approximate transport balance, considering the 0–500-m water column, we may infer that about two-thirds of the SEC that passes through the northern segment (Figure 10) feeds the NBC/NBUC. For instance, the annual mean zonal inflow entering the northern segment is 8.8 Sv, and

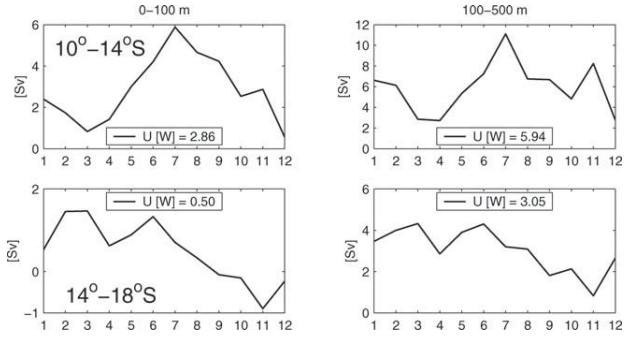

Figure 10. Annual cycle of the monthly mean net transport (Sv) estimates along the two meridional sections at 34°W. The top panels represent the northern segment (14°S to 10°S), and the bottom panels represent the southern segment (18°S to 14°S). Westward transport is positive. The left panels represent the surface layer (0–100 m), and the right panels represent the subsurface layer (100–500 m). The annual mean net transport is indicated inside the boxes. 1 Sv = 10^6 m^3 s^{-1}.

the increment in the northward transport from 14°S (12.8 Sv) to 10°S is of 5.6 Sv, reaching a total of 18.4 Sv. The remaining one-third of the SEC zonal transport goes to the BC flow, whose increment in the southward transport from 10°S (1.1 Sv) to 14°S is about 2.9 Sv, reaching a total value of 4.0 Sv.

At 14°S, the transport cycle along the year presents a different character from the surface to the subsurface layer. At the surface layer, a bimodal seasonal signal suggests an alternate dominance of the circulation, with the NBUC flow dominating from April to September and the BC flow dominating from October to March. Therefore, periods of maximum mean transport of the BC are associated with minimum transport of the NBUC. For August and September the dominance is not clear. At the subsurface layer, the NBUC resembles a normal distribution, with the maximum mean occurring in July. In this layer, the southward transport shows an increment trend in December and a secondary peak in March, in agreement with the top layer behavior.

The 18°S section is the first section to present a clear dominance of the BC flow, at the surface layer, throughout the year. This flow presents an annual mean of 2.8 Sv, reaching as much as 5 Sv in February. At the subsurface layer, the NBUC, although weaker when compared with the sections further north, is still dominant along the year.

Again, by applying an approximate transport balance, considering the 0–500-m water column, we may have an estimate of the SEC zonal inflow through the southern segment (Figure 10). The annual mean zonal inflow from 18°S to 14°S is 3.6 Sv. The increment in the northward transport from 18°S to 14°S is 2.4 Sv, reaching an annual value of 12.8 Sv at 14°S. The BC flow presents a flow increment of 1.9 Sv from 14°S to 18°S, reaching a total value of 5.9 Sv at 18°S. Although this estimate shows an unbalance of the order of 0.8 Sv, the results suggest that at this latitude range, the SEC divergence shows the tendency to feed evenly both the northward and the southward flows.

Furthermore, the EBM presents an intense spatial variability, presenting many circulation cells, whose interaction with the main field was also registered on our transport estimates. This spatial variability will be discussed in the next section.

SPATIAL VARIABILITY AND DYNAMIC PROVINCES

In order to look at the EBM spatial variability, mean temporal fields were computed for the sea surface height and for the flow pattern at both the surface (comprising mostly the TW) and subsurface (comprising mostly the SACW) layers (Figure 11). For instance, the mean field for January is dominated by an irregular flow pattern, where a succession of cyclonic and anticyclonic mesoscale gyres promotes intense cross-shelf water exchanges.

Considering the dynamic structures observed on a spatial and a seasonal perspective, we may divide the EBM in three dynamic provinces. The northern province, from 8°S to 13°S, is marked by a cyclonic circulation cell with a low sea-level signature in the center. The life cycle of this feature is very clear in the plots for July and October (Figure 11g,h,j,k). On an annual basis (not all months are shown), this structure starts to develop in May, gets very intensified and almost stationary

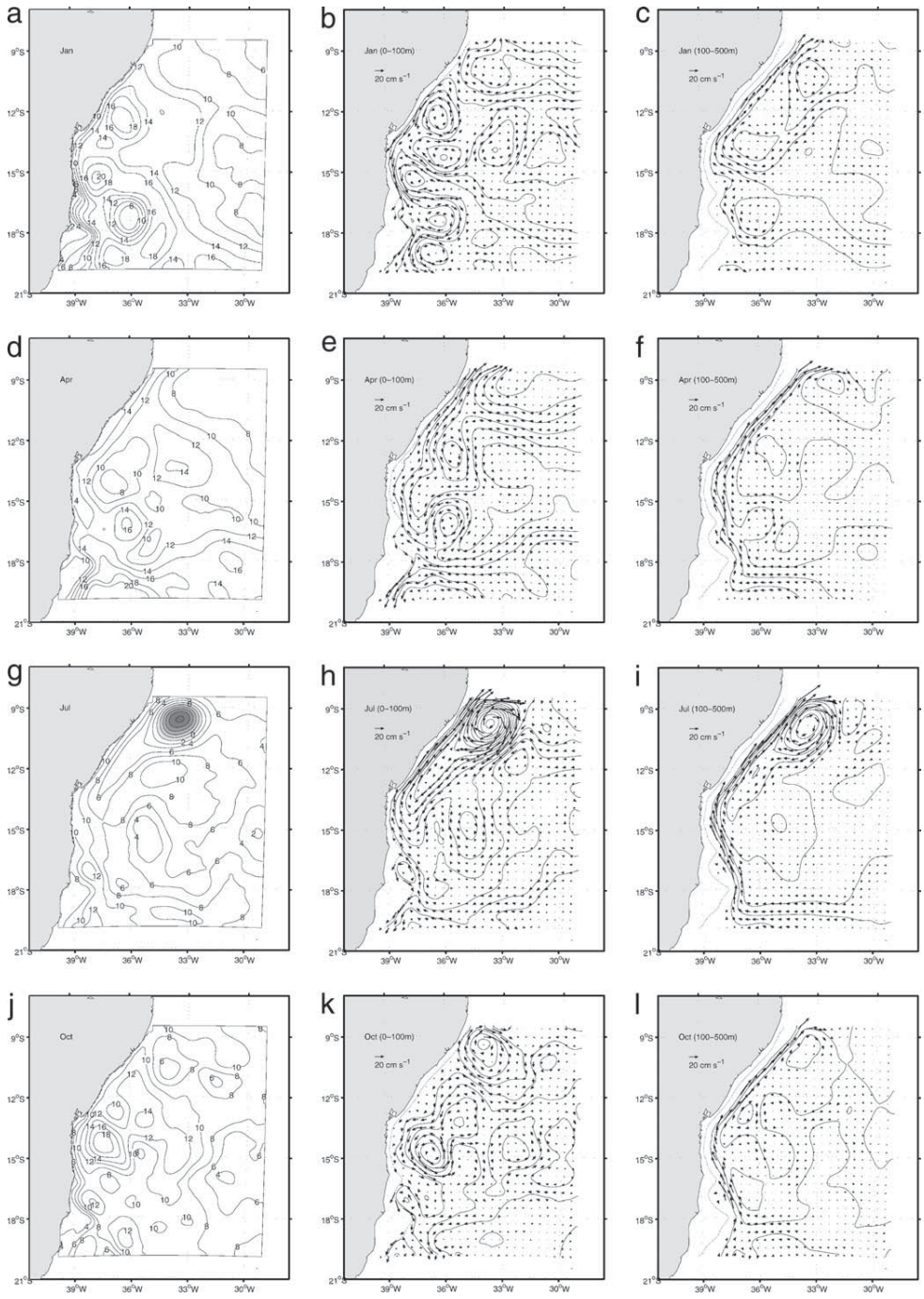

Figure 11. Monthly mean horizontal distribution of (a) the sea surface height (cm) and the integrated flow field for two distinct vertical layers (b) 0–100 m and (c) 100–500 m. From top to bottom, months are January, April, July, and October. Superposed solid contours on (b) and (c) represent the stream function patterns. The dotted line on those plots indicates the 200-m isobath.

from June to September, and loses its signature gradually in October and November.

The middle province, located from 13°S to 16°S (on the oceanic zone comprised between the cities of Salvador and Ilhéus) is characterized by two distinct and well-defined flow regime during the year. From October to March, the main flow is dominated by the southward flowing BC (see Figure 9 for the mean monthly transports and Figure 11b,k for the

flow fields for January and October), while from April to September, the NBUC northward flow is dominant (see Figure 11e,h for the mean monthly fields for April and July). A less marked transitional flow pattern is revealed in April, August, and September. It is important to remember that for the BC, most of the flow is confined to the top 100 m. The shelf width in this region is very narrow, and the coastal circulation is shown to be closely tied to the oceanic mesoscale processes, with intensification or flow reversals being associated with these features. The knowledge of such variability is particularly important here since the region between the bays (BTS and CMB in Figure 1) is very relevant to fishery and oil activities.

The southern province, from 16°S to 20°S, is marked by an extended and irregular shelf, developed between two major banks, the Royal Charlotte bank (16°S) and the Abrolhos bank (Figure 1). This irregular topography constrains and alters the flow, inducing spatial variability in physical, chemical, and biological features over the shelf (Knoppers, Ekau, and Figueiredo, 1999) and in adjacent oceanic waters.

Pereira *et al.* (2005) found an evidence of cross isobath residual barotropic currents due to tide interaction with topography. The authors reported that this process was particularly important on the southern flanks of the Abrolhos banks, where the tidal ellipses associated with the northern propagation of the barotropic tide were perpendicular to the slope of the flanks. The result for this interaction was the generation of upwelling favorable areas on the southern part of the flank and downwelling favorable areas on the northern flanks. Upwelling and downwelling were also modeled along the flanks on the Royal Charlotte bank, although not as intensely as those found on the sides of Abrolhos bank (Pereira *et al.,* 2005). Our model includes no tidal forcing, and relatively cooler and fresher water was a recurrent feature on the shallow areas around Abrolhos bank, suggesting that it is associated with the upwelling process. Additionally, the surface flow is southward oriented throughout the year (Figure 11b,e,h,k), an indication of a perennial BC flow at this latitude. From September to April, a flux divergence, shifting between 17°S to 19°S with resultant flow toward the south, represents an intensification on the BC flow.

When considering the three regions together, the flow patterns on the EBM appear to be in close agreement with the annual pattern for the trade winds, the prevailing wind system on the tropics. The trade winds are associated with the dynamics of the high pressure South Atlantic Anticyclone, blowing from E and NE during spring and summer (October to March), when the South Atlantic Anticyclone cell is displaced toward the S, and from SE during autumn and winter (April to September), when the anticyclone is at its northernmost position (Nimer, 1989). Accordingly, Rodrigues, Rothstein, and Wimbush (2007) state that positive (negative) wind stress curl produces an anomalous anticyclonic (cyclonic) circulation, whose southward (northward) component near the western boundary causes the SEC bifurcation to occur at a lower (higher) latitude during austral spring/summer (winter) months. Therefore, and in agreement with Rodrigues, Rothstein, and Wimbush (2007), our results show that during austral summer, when the SEC bifurcation occurs at a lower latitude, an intensification on the southward BC transport is observed, while during austral winter, when the SEC bifurcation occurs at a higher latitude, an intensification of the northward NBUC transport occurs.

EDDY INTERACTIONS IN THE EBM

The model results reveal an intense mesoscale activity along the EBM. These mesoscale features coexist with the large-scale circulation, may evolve into eddies and, in such cases, have a certain life time and a translation character. In this section, we discuss the behavior of a cyclonic and an anticyclonic eddy, detached from the main flow along a modeled annual cycle. Although mesoscale features are recurrent in all years of the model results, here, and for a qualitative analysis, we only discuss the model results for the fifth MG year cycle as reference.

We start our description with the cyclonic eddy (Figure 12) formed at the offshore region just north of the Abrolhos bank (18°S). The origins of this feature involve the interaction with two neighboring anticyclonic eddies (Figure 12a). The most important contribution comes from the northern eddy, which approaches from the upper limit of the Royal Charlotte bank (16°S) and favors an intense zonal flow. Owing to local bathymetric constraints, this eddy plunges parcels of shelf waters toward deep waters (Figure 12a). On its origin, the cyclonic eddy incorporates cooler, coastal upwelled water (surface temperature in the coastal vicinity over the Abrolhos bank is around 24°C, whereas the adjacent oceanic waters is around 28°C). After being formed, the cyclonic eddy is individualized and remains almost stationary for more than a month (Figure 12b). After that, it shows a translation character and rapidly propagates northward. At this point, the feature experiences a reorganization, assuming an elliptical shape (Figure 12c), and it is finally observed at the northern part of the EBM in the middle of June (Figure 12d). A composite altimetric image from AVISO in the middle of April 2004, and the calculated geostrophic field associated with it (Figure 12e), which resembles the geneses presented in Figure 12a, is used to illustrate the occurrence of such process in the region, showing compatible length and time scales.

The second pattern described here is related to the anticyclonic eddy (Figure 13). The formation of this feature was traced back to August, at around 12°S (Figure 13a). The feature propagates southward, following the main flow for a period of a month or so (Figure 13b), when it then interacts with the shelf region and appears better individualized and intensified during the period of October/November (Figures 13c,d). In analogy to what was presented for the cyclonic feature, a composite altimetric image for the middle of September 2004 with the associated calculated geostrophic distribution (Figure 13e) presents a well-defined anticyclonic eddy, north of 16°S, adding physical evidence to our model results.

It is important to emphasize that, for either case, our description is focused on the major feature and its related translation pattern. Less important features, sometimes presenting erratic patterns, have also been observed.

On our model results, a typical southward extension for the anticyclonic feature is coincident with the region limited by the

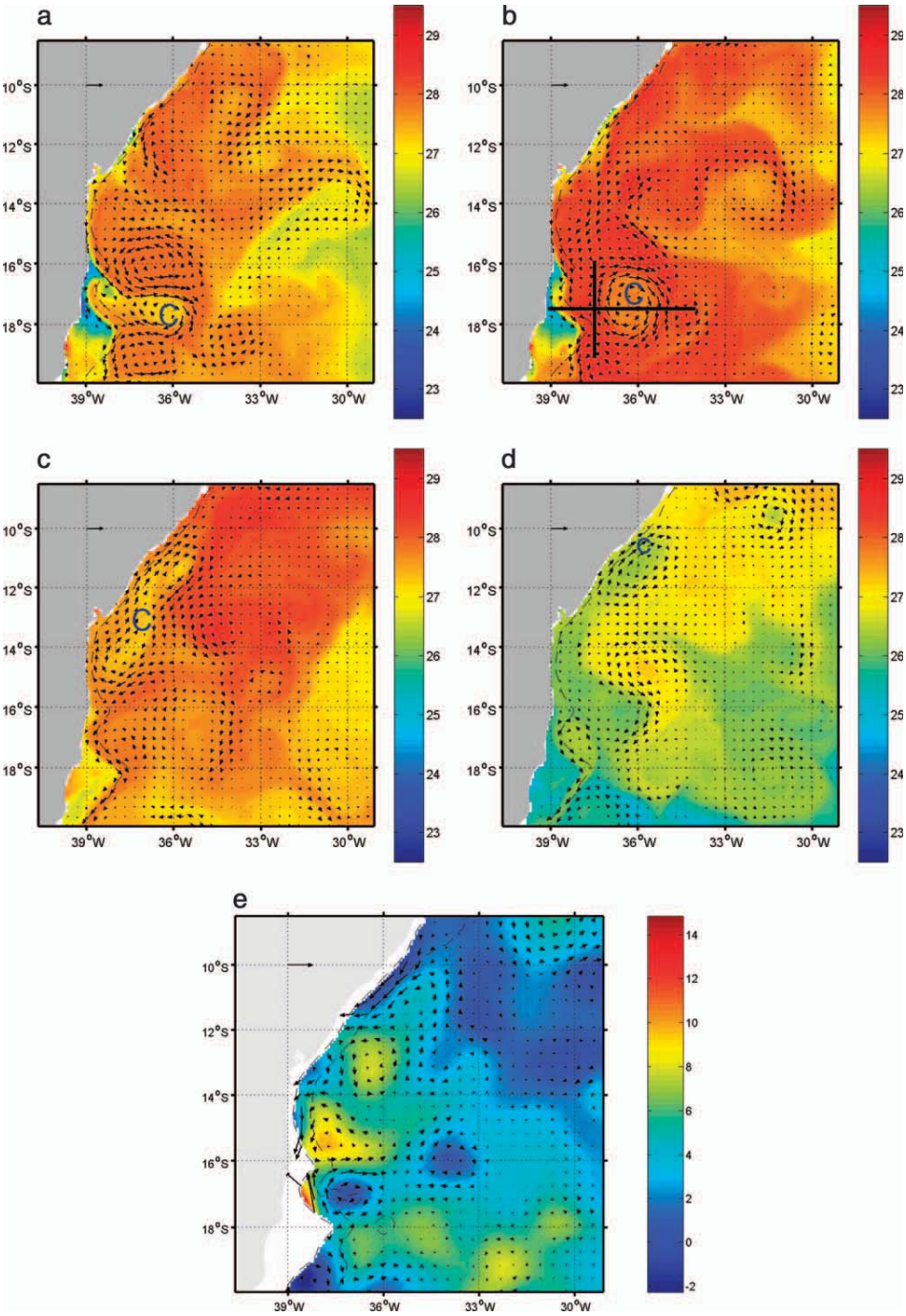

Figure 12. The geneses and life cycle of a modeled cyclonic system (designated with the letter C) on the EBM during an annual cycle and based on the 10-d averages of the horizontal velocity and temperature distribution at 10 m. (a) Middle of January, (b) middle of February, (c) end of April, (d) middle of June. (e) A composite altimetric image from AVISO data set and its calculated geostrophic field distribution for the middle of April 2004. The vector scale is 1 m s^{-1}.

northern flank of the Abrolhos bank, which is also the origin region for the cyclonic feature. The translation patterns appear to be temporally connected to the intensification of the main seasonal EBM flow patterns, with the cyclonic northward translations occurring preferentially in the first half of the year (when the NBUC starts to intensify) and the anticyclonic southward propagation occurring in the second half of the year (when the BC starts to intensify).

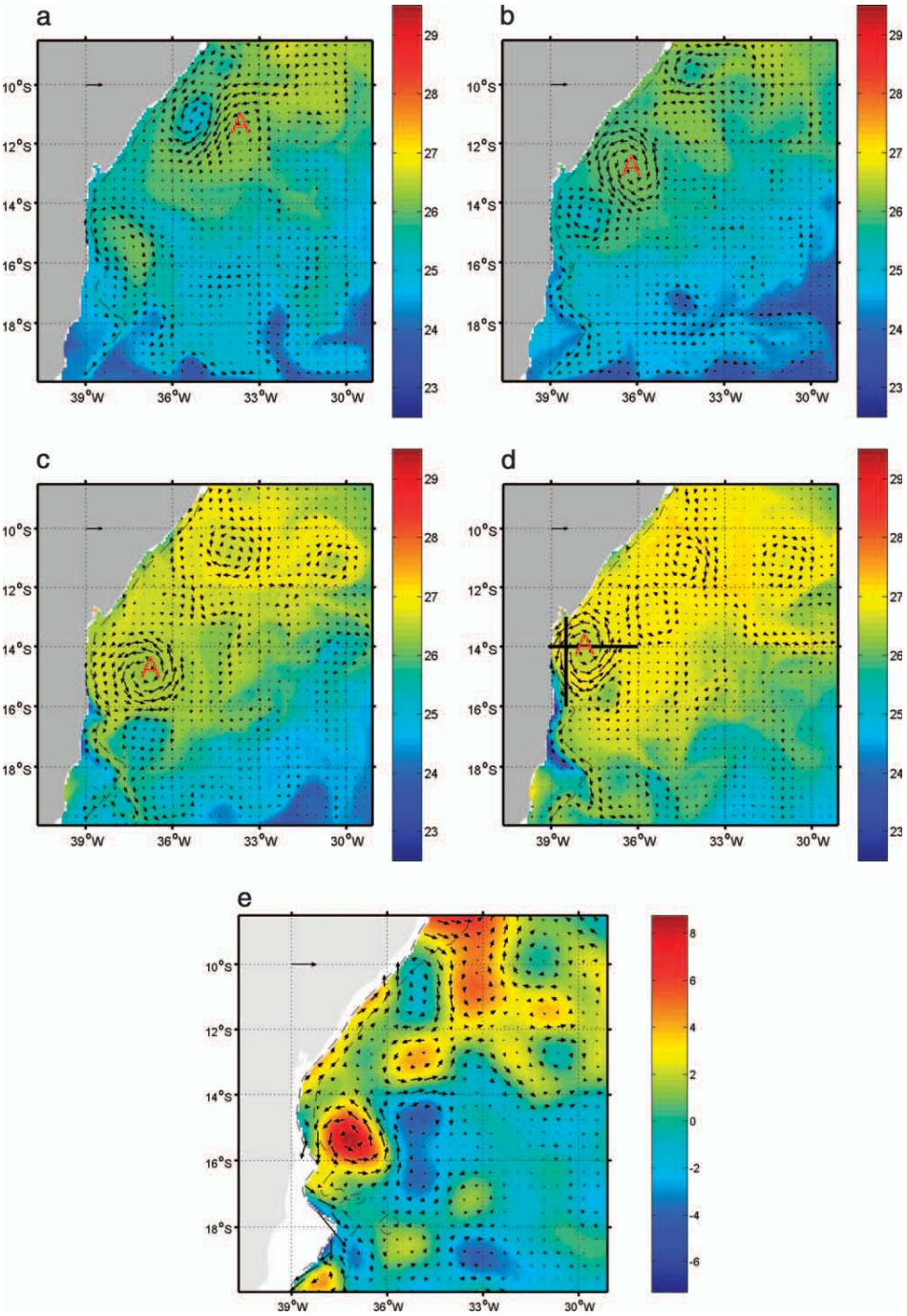

Figure 13. The geneses and life cycle of a modeled anticyclonic system (designated with the letter A) on the EBM during an annual cycle and based on the 10-d averages of the horizontal velocity and temperature distribution at 10 m. (a) beginning of August, (b) middle of September, (c) end of October, and (d) middle of November. (e) A composite altimetric image from AVISO data set and its calculated geostrophic field distribution for the middle of September 2004. The vector scale is 1 m s^{-1}.

On their pathways, these features interact with the near-shelf region. Their dynamic structure during such events, the cyclonic eddy during mid-February (Figure 12b), and the anticyclonic eddy during mid-November (Figure 13d) are explored in two specific subsections. Our aim here is to foster new ideas on the EBM near-shelf dynamics, especially regarding the effects of the remote forcing on the local circulation.

Furthermore, Campos (2006) invokes a possible northward

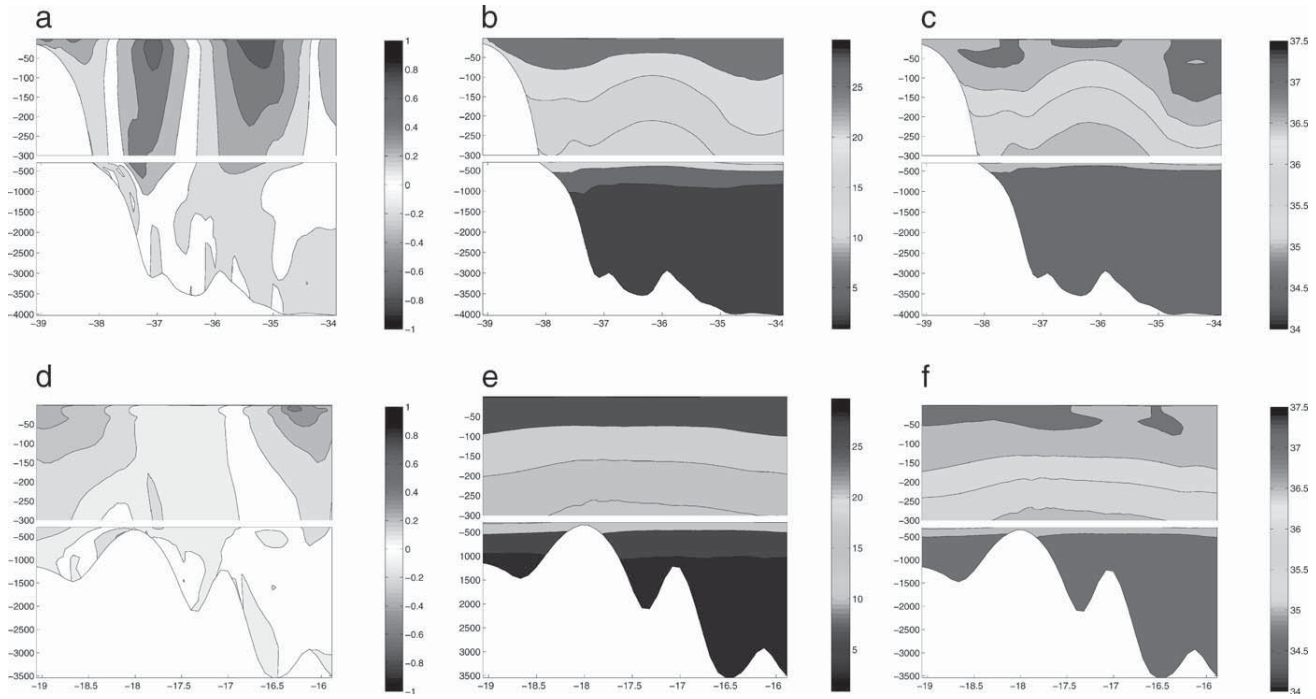

Figure 14. Latitudinal (top) and Meridional (bottom) sectional structure for (a) velocity, (b) temperature, and (c) salinity along a modeled cyclonic (clockwise) eddy on the EBM, in the middle of February. The locations of these sections are represented in Figure 12b.

propagation behavior for the cyclonic Vitória eddy. Our MG domain (Figure 2) does not extend south of the Abrolhos banks, where the Vitória eddy has been experimentally reported (Schmid *et al.,* 1995). An extra experiment set, however, with a larger domain (not shown), has shown evidence of a recurrent Vitória eddy south of the Abrolhos banks as well as the mesoscale dynamics described above. According to our analysis, these features may not refer to a northward propagation of the Vitória eddy, but as mesoscale features, formed north of 19°S, that indeed presents a seasonal propagation character.

Snapshot over a Cyclonic Eddy

In the middle of February, a mesoscale cyclonic eddy appeared well developed, centered at ~17.25°S and 36.25°W (Figure 12b), in the offshore waters adjacent to Abrolhos bank. At that time, the eddy was cyclonic (clockwise), associated with a negative sea surface height reaching up to 11 cm on the core. It had a 130-km diameter, remaining stationary for a few days. At 10-m depth, it presented a maximum cross-shore (u) velocity component of 0.85 m s^{-1} eastward at its northern limit (16.25°S) and of 0.95 m s^{-1} westward at its southern limit (18.25°S). The alongshore velocity component (v) reached 0.83 m s^{-1} southward at the eastern limit (35.25°W) and 0.71 m s^{-1} northward at the western limit (37.25°W).

Figure 14 shows the latitudinal (top panels) and meridional (bottom panels) sections of the velocity structure and the associated hydrographic properties. The isotherms (Figure 14b) and isohaline contours (Figure 14c) are tilted upward in the center of the eddy, suggesting an eddy induced upwelling, whose effect extends over the 500-m depth. On the coast side of the eddy, a prograding front, observed on the hydrographic sections, suggests that offshore water is brought to the shelf domain, a possible combined effect of the coastal upwelling process and the cyclonic translation. The divergence of the surface layers also favors the southward near-shelf flow (Figure 14a), inducing an intense zonal flow and a sharp flow gradient with the cyclonic eddy itself.

Snapshot over an Anticyclonic Eddy

In the middle of November, a mesoscale eddy appeared at ~14.00°S and 37.75°W, in the vicinity of Baía de Camamu and Baía de Todos os Santos, the two major coastal systems on the EBM (Figure 13d). This eddy was anticyclonic (anticlockwise), reaching a positive sea surface height of 25 cm at the core. It presented an elliptical shape on its surface, with a minor latitudinal axis of ~175 km and a major longitudinal axis of ~250 km. At 10-m depth, the velocity field extended to a diameter of ~270 km and assumed a more regular shape. The eddy presented a maximum cross-shore (u) velocity component of 0.8 m s^{-1}, westward at its northern limit (13°S), with highest intensity over the shelf. At its southern limit (15°S), the highest velocity was also of 0.8 m s^{-1} eastward, around 38.25°W. The alongshore velocity revealed a pronounced asymmetry, with the alongshore (v) component reaching 1.2 m s^{-1}, southward,

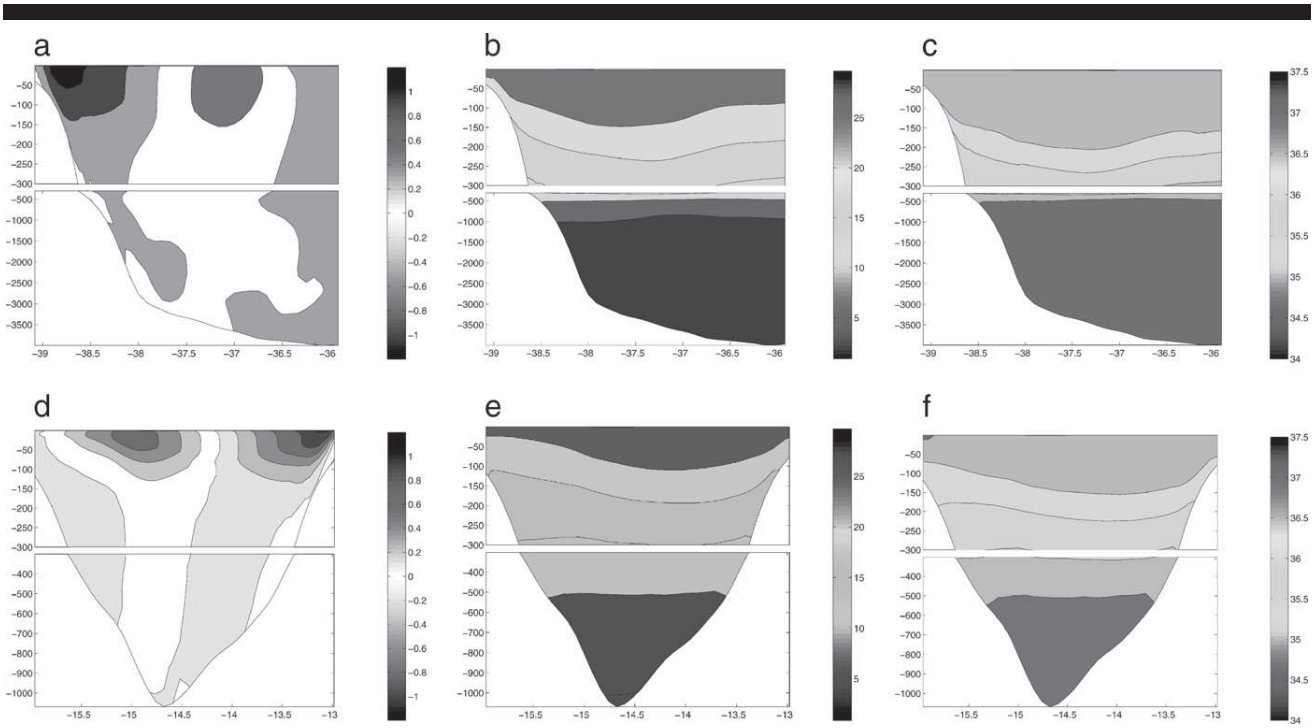

Figure 15. Latitudinal (top) and Meridional (bottom) sectional structure for (a) velocity, (b) temperature, and (c) salinity along a modeled anticyclonic (anticlockwise) eddy on the EBM, in the middle of November. The locations of these sections are represented in Figure 13d.

over the shelf, at the westernmost limit (38.85°W) and 0.8 m s^{-1}, northward, at the eastern limit(37.00°W).

The sections presented in Figure 15 for the latitudinal (top panels) and meridional (bottom panels) axis of the eddy reveal some possible connections of the anticyclonic feature with the regional dynamics. The isotherms (Figure 15b) and isohaline contours (Figure 15c) are tilted downward in the center of the eddy, suggesting a downwelling process, whose effect extends to depths over 200 m. On the near coast side of the eddy, an asymmetric alongshelf flow structure and a pronounced near coast tilting up for the hydrographic properties are noticeable, suggesting water renewal, a possible result of the meander coupling with the coastal dynamics.

Connections of eddies with the upwelling coastal system have been studied on the SE coast of Brazil (Calado, Gangopadhyay, and da Silveira, 2006). Asymmetries on the eddy structure were associated with such interactions. Feedback mechanisms with the coastal processes are likely to happen in the EBM. The very intense alongshore and sharp flow gradients associated with the meandering structures may be enhancing shelf-edge upwelling that, in turn, contributes to maintain the flow structure gradient.

CONCLUDING REMARKS

In this work, an effort was made to evaluate the main circulation patterns of the EBM, focusing on its seasonal variability and on the interaction between mesoscale features, the mean flow, and the associated coastal region. The circulation in the area has been shown to be markedly influenced by the large-scale circulation driven by the SEC divergence. The SEC represents the northern limb of the South Atlantic Subtropical Gyre, a large-scale feature, which, if not specified properly at the boundary, imposes the first problem for a regional circulation model. To cope with this difficulty, we adopted the nesting capability integrated into the Regional Ocean Modeling System (ROMS), retaining on the regional solution the connections and forcing from the large-scale circulation.

In order to validate our modeling system, in a region where the data are scarce and irregularly sampled in space and time, we made use of eddy kinetic energy estimates from satellite altimetry. Our validation procedure revealed that for the EBM zone (8°S to 20°S) there is a reasonable agreement between the mean model outputs and the satellite data. On higher energetic zones though, such as the low latitude equatorial zone or the Brazil/Malvinas Confluence zone, the model had the tendency to underestimate the ocean variability. The modeled results were also compared with the few observations available for the region, and the transports obtained were compatible with those found in the literature. Based on the results above, we believe that the nesting technique adopted here has proved to be adequate and realistic to study the circulation on the EBM.

The EBM not only has a complex dynamics, but it also hosts some of the most important coastal and biological systems along the Brazilian coast, such as the coral reef aggregation on

the Abrolhos bank region or the two major bay systems: Baía de Todos os Santos and Baía de Camamu. Apart from Stramma, Ikeda, and Peterson (1990) and Rodrigues, Rothstein, and Wimbush (2007), and prior to this work, the EBM dynamic connectivity was virtually unknown.

The EBM is divided into three zones, according to their distinct seasonal dynamic features. These zones were geographically defined as the northern province (8°S to 13°S), the middle province (13°S to 16°S), and the southern province (16°S to 20°S). The results have shown that the provinces are seasonally connected either by the mean flow or by the mesoscale variability on the flow.

The permanent mean flow is deeply influenced by the divergence of the southern branch of the SEC, which is responsible for feeding the major western boundary currents, known as the Brazil/North Brazil Current system. For the surface layer (0–100 m) and at the northern province, the NBUC is the main dynamic permanent feature (annual mean transport of 3.2 Sv), while the BC is just a thin flow confined to the top few meters (annual mean transport of 0.5 Sv). As we move southward, the BC deepens and its transport is intensified. In the middle province, the dominance of the surface layer circulation seasonally alternates between the southward BC flow (annual transport of 2.4 Sv) and the northward NBUC flow (annual transport of 2 Sv), while around the Abrolhos bank, in the southern province, the BC appears as the dominant surface feature (annual transport of 2.8 Sv) and has a perennial character.

In subsurface waters (100–500 m), the NBUC connects the EBM continuously, with the annual mean transport increasing northward from 8.5 Sv (18°S) to 15 Sv (10°S), while the southward BC flow increases in a reverse manner, from 0.5 Sv (10°S) to 3 Sv (18°S). Considering the surface and the subsurface layers together and on an annual basis, our results also show that the SEC has a different contribution into the BC/NBC system according to the region. In the northern part of the domain (10°S to 14°S) only one-third of this zonal flow feeds the BC, while the remainder is incorporated into the NBUC flow. In the southern part of the domain (14°S to 18°S) this relation reaches an almost even balance.

When considering the three provinces together, the flow patterns on the EBM appear to be in close agreement with the annual cycle for the trade winds, the prevailing wind system for the tropics. Our results show that during austral spring and summer (when E and NE winds prevail), the SEC bifurcation occurs at a lower latitude, and an intensification of the southward BC transport is observed. During austral autumn and winter (when SE winds prevail), the SEC bifurcation occurs at a higher latitude, and an intensification of the northward NBUC transport occurs. Our results are in agreement with the pattern proposed by Rodrigues, Rothstein, and Wimbush (2007) for the SEC divergence.

The regional simulation reveals intense mesoscale activities. Well-defined cyclonic and anticyclonic eddies detached from the main flow are seen translating throughout the domain along the year. The translations of these features are connected to the seasonal main EBM flow, with cyclonic (anticyclonic) eddies preferably translating northward (southward) along the first (second) semester of the year. The physics involved in this dynamics are far beyond the scope of this work and remain an open issue that should be properly addressed in a future work.

Modeling evidence of eddy interaction with the near-shelf dynamics is presented for both cases. Such direct connections have never been reported in the zone, but Gaeta *et al.* (1999) report evidence of offshore-shelf fertilization associated with the Vitória eddy, south of the Abrolhos bank. Considering that tropical shelves governed by western boundary currents are the least productive ocean margins of the world, unless land runoff and eddy induced shelf-edge upwelling become significant (Walsh, 1988), the EBM eddy interaction may have environmental relevance in the oligotrophic EBM dynamics. Further validation efforts should be pursued.

ACKNOWLEDGMENTS

The authors appreciated the constructive criticism from the anonymous reviewers of this work. Lúcio Figueiredo Rezende acknowledges support from Programme Alßan, the European Union programme of high level scholarships for Latin America (Grant E04D028784BR) and Mauro Cirano was supported by a CNPq Research grant.

LITERATURE CITED

Agência Nacional de Petróleo (ANP), 2009. Agência Nacional de Petróleo. Ministério de Minas e Energia. http://www.brasil-rounds.gov.br (accessed October 25, 2010).

Backeberg, B.C., 2006. *Mesoscale Variability Study of the Agulhas Current from Satellite Radar Altimetry and a High Resolution Model*. Bergen, Norway: University of Bergen, 42p.

Brachet, S.; Le Traon, P.Y., and Le Provost, C., 2004. Mesoscale variability from a high-resolution model and from altimeter data in the North Atlantic Ocean. *Journal of Geophysical Research,* 109, C12025.

Calado, L.; Gangopadhyay, A., and da Silveira, I.C.A., 2006. A parametric model for the Brazil Current meanders and eddies off Southeastern Brazil. *Geophysical Research Letters,* 33, L12602. doi:10.1029/2006GL026092.

Campos, E.J.D., 2006. Equatorward translation of the Vitoria Eddy in a numerical simulation. *Geophysical Research Letters,* 33, L22607.

Carton, J.A.; Chepurin, G., and Cao, X., 2000. A simple ocean data assimilation analysis of the global upper ocean 1950–95. Part II: Results. *Journal of Physical Oceanography,* 30, 311–326.

Carton, J.A.; Chepurin, G.; Cao, X., and Giese, B., 2000. A simple ocean data assimilation analysis of the global upper ocean 1950–95. Part I: Methodology. *Journal of Physical Oceanography,* 30, 294–309.

Castro, B.M. and Miranda, L.B., 1998. Physical oceanography of the western Atlantic continental shelf located between 4°N and 34°S coastal segment (4,*W*). *In:* Robinson, A.R. and Brink, K.H. (eds.), *The Sea*, vol. 11, pp. 209–251. New York: Wiley.

Cirano, M.; Mata, M.M.; Campos, E.J.D., and Deiró, N.F.R., 2006. A circulação oceânica de larga-escala na região oeste do Atlântico Sul com base no modelo de circulação global OCCAM. *Revista Brasileira de Geofísica,* 24, 209–230 [In Portuguese].

Da Silva, A.; Young, A.C., and Levitus, S., 1994. Atlas of Surface Marine Data 1994, Volume 1: Algorithms and Procedures. NOAA Atlas NESDIS 6. Silver Spring, Maryland: U.S. Department of Commerce, National Oceanic and Atmospheric Administration.

Ducet, N.; Le Traon, P. Y., and Reverdin, G., 2000. Global high-resolution mapping of ocean circulation from TOPEX/Poseidon and ERS-1 and -2. *Journal of Geophysical Research,* 105(C8), 19477–19498.

Ekau, W. and Knoppers, B. 2003. A review and redefinition of the large marine ecosystems of Brazil. *In:* Sherman, K. and Hempel, G.

(eds.), *Large Marine Ecosystems of the World—Trends in Exploitation, Protection and Research*. Amsterdam: Elsevier Science.

Emilsson, I., 1961. The shelf and Coastal waters off southern Brazil. *Boletim do Instituto Oceanográfico de Universidade São Paulo,* 17(2), 101–112.

Evans, D.L.; Signorini, S.S., and Miranda, L.B., 1983. A note on the transport of the Brazil Current. *Journal of Physical Oceanography,* 13(9), 1732–1738.

Gaeta, S.A.; Lorenzetti, J.A.; Miranda, L.B.; Susini-Ribeiro, S.R.M.; Pompeu, M., and Araujo, C.E.S., 1999. The Vitória eddy and its relation to the phytoplankton biomass and primary productivity during austral fall of 1995. *Archive of Fishery and Marine Research,* 47(2/3), 253–270.

Haidvogel, D.B.; Arango, H.G.; Hedstrom, K.; Beckmann, A.; Malanotte-Rizzoli, P., and Shchepetkin, A.F., 2000. Model evaluation experiments in the North Atlantic Basin: simulations in nonlinear terrain-following coordinates. *Dynamics of Atmospheres and Oceans,* 32, 239–281.

Knoppers, B.; Ekau, W., and Figueiredo, A.G., 1999. The coast and shelf of east and northeast Brazil and material transport. *Geo-Marine Letters* 19(3), 171–178. DOI:10.1007/s003670050106 (accessed October 25, 2010).

Large, W.G.; McWilliams, J.C., and Doney, S.C., 1994. Oceanic vertical mixing: a review and a model with a nonlocal boundary layer parameterization. *Reviews of Geophysics,* 32, 363–403.

Leão Z.M.A.M., 2002. Abrolhos—o complexo recifal mais extenso do oceano Atlântico Sul. *In:* Schobbenhaus, C.; Campos, D.A.; Queiroz, E.T.; Winge, M., and Berbert-Born M. (eds.), *Sítios Geológicos e Paleontológicos do Brasil*, 1 ed. Brasilia: Departamento Nacional de Produção Mineral (DNPM), Comissão Brasileira de Sítios Geológicos e Paleobiológicos (SIGEP), 2002, v.01, pp. 345–359. [In Portuguese].

Lessa, G.; Dominguez, J.M.L.; Bittencourt, A.C.S.P., and Brichta, A., 2001. The tides and tidal circulation of Todos os Santos Bay, Northeast Brazil: a general characterization. *Anais da Academia Brasiliera de Ciências,* 73(2), 245–261.

Miranda, L.B. 1985. Forma de correlação T-S de massa de água das regiões costeira e oceânica entre o Cabo de São Tomé (RJ) e a Ilha de São Sebastião (SP), Brasil. *Boletim do Instituto Oceanográfico de Universidade São Paulo,* 33(2), 105–119 [In Portuguese].

Miranda, L.B. and Castro, B.M. 1982. Geostrophic flow conditions of the Brazil Current at 19°S. *Ciência Interamericana,* 22, 44–48.

Nimer, E., 1989. *Climatologia do Brasil*. Rio de Janeiro: Instituto Brasileiro de Geografia e Estatística, 421p [In Portuguese].

Penven, P. 2003. ROMSTOOLS user's guide. technical report, Instituit de Recherche pour le Développement, 213 rue Lafayette, Paris, France. http;//roms.mpl.ird.fr/ (accessed October 25, 2010).

Penven, P.; Debreu, L.; Marchesiello, P., and McWilliams, J.C., 2006. Evaluation and application of the ROMS 1-way embedding procedure to the central California upwelling system. *Ocean Modelling,* 12, 157–187.

Penven, P.; Echevin, V.; Pasapera, J.; Colas, F., and Tam, J., 2005. Average circulation, seasonal cycle, and mesoscale dynamics of the Peru Current System: a modeling approach. *Journal of Geophysical Research,* 110, C10021.

Pereira, A.; Belém, A.L.; Castro, B.M., and Geremias, R., 2005. Tide-topography interaction along the eastern Brazilian shelf. *Continental Shelf Research,* 25, 1521–1539.

Reid, J.L., 1989. On the total geostrophic circulation of the South Atlantic Ocean: flow patterns, tracers and transports. *Progress in Oceanography,* 23, 149–244.

Rezende, L.F., 2001. Estimativa dos padrões de circulação oceânica superficial baseado no lançamento de corpos de deriva e em derramamentos ocorridos no litoral sul do estado da Bahia. *Revista Tecnologia e Ambiente,* 7, 73–89 [In Portuguese].

Rodrigues, R.R.; Rothstein, L.M., and Wimbush, M., 2007. Seasonal variability of the south equatorial current bifurcation in the Atlantic Ocean: a numerical study. *Journal of Physical Oceanography,* 37, 16–30.

Saraceno, M.; Provost, C.; Piola, A.R.; Bava, J., and Gagliardini, A., 2004. Brazil Malvinas frontal system as seen from 9 years of advanced very high resolution radiometer data. *Journal of Geophysical Research,* 109, C5.

Schmid, C.; Schäfer, H.; Podestá, G., and Zenk, W., 1995. The Vitória Eddy and its relation to the Brazil Current. *Journal of Physical Oceanography,* 25, 2532–2546.

Schott, F.A.; Dengler, M.; Zantopp, R.; Stramma, L.; Fischer, J., and Brandt, P., 2005. The shallow and deep western boundary circulation of the South Atlantic at 5°–11°S. *Journal of Physical Oceanography,* 35, 2031–2053.

Schott, F.A.; Fischer, J., and Stramma, L., 1998. Transports and pathways of the upper-layer circulation in the western tropical Atlantic. *Journal of Physical Oceanography,* 28(10), 1904–1928.

Shchepetkin, A.F., and McWilliams, J.C., 2005. The Regional Oceanic Modeling System (Roms): a split-explicit, free-surface, topography-following-coordinate oceanic model. *Ocean Modelling,* 9, 347–404.

Silveira, I.C.A.; Miranda, L.B., and Brown, W.S., 1994. On the origins of the North Brazil Current. *Journal of Geophysics Research,* 99, 22501–22512.

Silveira, I.C.A.; Schmidt, A.C.K.; Campos, E.J.D.; Godoi, S.S., and Ikeda, Y., 2000. A Corrente do Brasil ao largo da costa leste brasileira. *Revista Brasileira de Oceanografia,* 48(2), 171–183 [In Portuguese].

Souza, T.C.M. and Petrere Júnior, M. 2008. Characterization of small-scale fisheries in the Camamu-Almada basin, southeast state of Bahia, Brazil. *Brazilian Journal of Biology* [online], 68, 711–719. doi: 10.1590/S1519-69842008000400005 (accessed October 25, 2010).

Stramma, L. and England, M., 1999. On the water masses and mean circulation of the South Atlantic Ocean. *Journal of Geophysical Research,* 104(C9), 20,863–20,883.

Stramma, L.; Ikeda, Y., and Peterson, R.G., 1990. Geostrophic transport in the Brazil Current region north of 20°S. *Deep-Sea Research,* 37(12), 1875–1886.

Stramma, L. and Schott, F. 1999. The mean flow field of the tropical Atlantic Ocean. *Deep-Sea Research, Part II,* 46, 279–303.

Teles-Machado, A.; Peliz, A.; Dubert, J., and Sánchez, R.F., 2007. On the onset of the Gulf of Cadiz Coastal Countercurrent. *Geophysical Research Letters,* 34, L12601.

U.S. Department of Commerce, National Oceanic and Atmospheric Administration (NOAA), 2001. Two-minute Gridded Global Relief Data (ETOPO2), technical report. National Geophysical Data Center. http://sos.noaa.gov/datasets/Land/etopo2.html (accessed October 25, 2010).

U.S. Department of Commerce, 2004. Large marine ecosystems of the world, technical report. National Oceanic and Atmospheric Administration. http://www.lme.noaa.gov/ (accessed October 25, 2010).

Walsh, J.J., 1988. *On the Nature of Continental Shelves*. San Diego: Academic Press, 520p.